Optimized Design of a Double-Shell Integrated Lens Antenna

Jorge R. Costa, Eduardo B. Lima and Carlos A. Fernandes
Instituto de Telecomunicações, IST, Av. Rovisco Pais, 1049-001 Lisboa, Portugal
Lisbon University Institute (ISCTE-IUL), DCTI, Av. das Forças Armadas, 1649-026 Lisboa, Portugal

***Abstract*- This communication presents a new double-shell integrated scanning lens antenna, based on the Bifocal and the Abbe sine condition approaches. The lens was designed using the authors optimized design rules described in [1]. The lens is intended to scan a high directivity beam within the [-16º, 16º] angular interval, with low gain scan loss at millimeter waves. Target specifications at 62.5 GHz are full beam width of 8º at -10 dB level (31 dBi directivity) and maximum gain scan loss lower than 1 dB. The lens diameter is 70 mm.**

I. Introduction

Integrated dielectric lens antennas have been used in several millimeter wave applications where they transform the feed radiation pattern into a prescribed shaped output radiation pattern. Integrated lens examples can be found for radio-astronomy [2], wireless communications [3]-[4], satellite communications [5], ultra-wideband communications (UWB) [6]-[7], etc. Integrated dielectric lenses can be used as scanning or multi-beam antennas: an array of feeds is integrated at the base of the lens to produce equal number of focused output beams, each one with a prescribed tilt angle. 2D lens antennas have been studied for scanning applications [8]-[9] but they only allow focusing the beam in one of the main planes. Alternatively, a full 3D lens can be use to shape the radiation pattern in both planes. Common integrated 3D scanning lenses are mostly based on canonical shapes like the extended hemispherical, hyper hemispherical or elliptical [10]-[12]. However, for increasing off-axis feed positions, the usual problem of beam degradation and increase of internal reflections cannot be mitigated during lens design process, since those canonical configurations have a fixed lens shape, not allowing its optimization. In [13], the authors have presented a shaped scanning lens with improved performance. However, the lens was designed using the Abbe sine condition from geometrical optics, where the important relation between the feed off-axis position and the off-set output angle is absent from the formulation. Therefore, a trial and error approach was necessary to find the best lens shape. Based upon a Bifocal design procedure, the authors were able to find a set of closed form expressions that relate the Abbe design parameters to the usual parameters of a scanning lens enabling a straightforward optimized design [1].

This communication presents a new double-shell integrated scanning lens antenna which was designed making use of the Abbe sine condition formulation for a double-shell lens, complemented with additional scanning information like the maximum feed off-set position and its associated scanning angle [1].

II. Lens Design

When designing axial-symmetric scanning lenses, a very common and well known design procedure is the Bifocal approach. The Bifocal design establishes a direct relation between two maximum focal points, $-a$ and a, with the direction of the exiting rays α, and $-\alpha$, see Figure 1. With this formulation, for a scanning angle comprised within $\pm\alpha$, the feed optimum location corresponds to a parabolic arc, centered at $(0, -\delta)$. The number of lens profile points obtained from the Bifocal design procedure is not user controlled, being dependent on the lens parameters. Generalization of the Bifocal design for a double-shell integrated lens shows that the number of points that define both surfaces becomes especially scarce. Interpolation is required to smooth the surface, but although good approximations can be achieved, the radiated rays accumulate residual refraction errors at the two lens interfaces, degrading the lens performance. The lens axial depth is defined by F and T, for the inner and outer shell height respectively.

As an alternative, the Abbe design approach allows obtaining a scanning lens with complete control over the number of points in the lens profile. Lens axial thickness is defined by $F_0 = F + \delta$ and T, for the inner and outer shell respectively, Figure 1. The Abbe sine condition is satisfied when the intersection points of the extended rays departing from the on-axis sensor and the corresponding extended transmitted rays all lie on a circumference centered at the sensor, with radius f_e [14]. The lens profile can be obtained with good accuracy, however the design does not involve explicitly any scanning design parameters, thus requiring a trial and error design sequence until the desired scanning conditions are met.

Because Abbe sine formulation parameters are not adequate for the design of an integrated scanning lens, an equivalence was developed between its design parameters and those from the Bifocal approach. Closed-form expressions for the lens design can be found in [1]; the same parameter naming is used in the present communication for convenience. The lens design and analysis were performed with the in-house ILASH software tool [15], which already includes the above mentioned lens formulation.

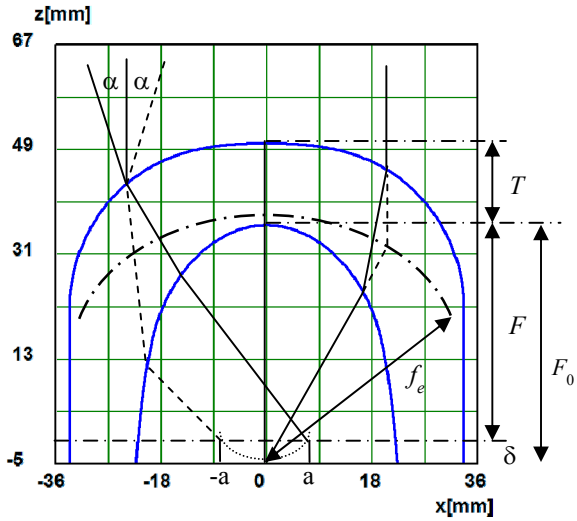

Figure 1. Self-standing double-shell scanning lens profile.

The lens is intended to produce multiple beams from 0º to 18º, corresponding to multiple positions of the feed at the base. Selected materials for the inner and outer shells are MACOR ($5.5 - j0.063$) and Polystyrene ($2.55 - j0.002$). The lens is fed by the same waveguide feed described in [13] for 62.5 GHz operation. For scanning the beam, the feed is displaced along the lens base in the H-plane. The scanning MACOR-Polystyrene lens dimensions $F = 36mm$ and $T = 14mm$ were chosen according to maximum available material diameter restrictions. For this material choice, the possible lenses and corresponding f_e values are presented in the $(a/F, \alpha)$ plane in Figure 2. For constant a value, the lenses with the larger radius and which normally suffer from lower internal reflections tend to be close to the red dashed line in Figure 2.

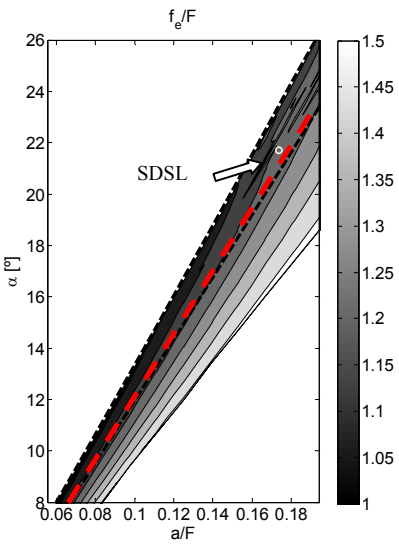

Figure 2. Range of $(a/F, \alpha)$ parameters for viable SDSL lenses, showing the correspondence with f_e/F parameter. Example for $\varepsilon_{r1} = 5.5$, $\varepsilon_{r2} = 2.53$, $T/F = 0.39$.

Based upon the inspection of some of those lenses with maximum scanning angle close to α = 20º, a lens profile was chosen, see Figure 1. Corresponding locus in the $(a/F, \alpha)$ plane is marked in Figure 2 with a white circle. The ray tracing of the scanning lens for the on-axis feed position and for the maximum feed displacement at $a = 6mm$ is presented in Figure 3.

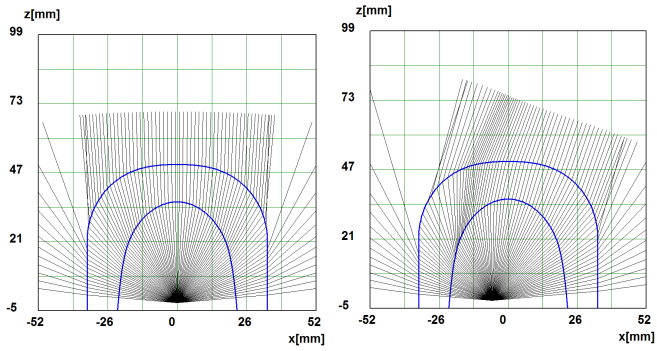

Figure 3. Ray tracing for on-axis feed position ($x = 0$) and for the maximum off-axis feed position ($x = 6\ mm$).

III. Lens Analysis

The simulated radiation patterns for the different feed positions are shown in Figure 4. All radiation patterns are referred to their maximum gain, enabling to observe gain scan loss.

The overall simulated performance of the lens is presented in Table I considering both the case with and without material losses. The gain increase towards off-axis position is explained by the fact that the linear (plane) path that was chosen for feed scanning is not coincident with the lens focal arc at the origin, but instead crosses it near $x = \pm 4.5\ mm$. This is a compromise scanning path that leads to the highest gain with minimum scan loss.

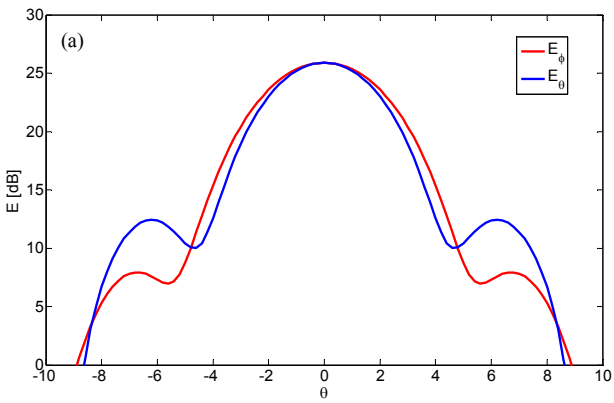

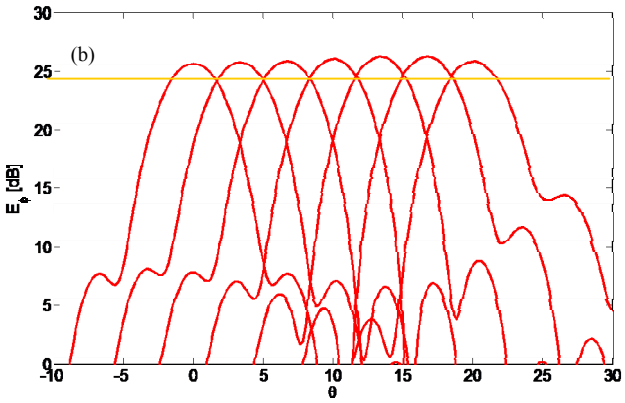

Figure 4. Imaging lens simulated radiation pattern with waveguide feed: a) on axis feed position, E-plane in blue and H-plane in red; b) H-plane radiation pattern for x = 0, 1, 2, 3, 4, 5 and 6 mm;

TABLE I
SCANNING LENS PERFORMANCE PARAMETERS

Feed position [mm]	θ_{max} [º]	without material loss			with material loss		
		D [dBi]	G [dBi]	η [%]	D [dBi]	G [dBi]	η [%]
x=0	0º	31.4	30.6	83.2	31.4	25.7	27.4
x=-1	3.5º	31.5	30.8	83.6	31.4	25.8	27.5
x=-2	6.5º	31.6	30.8	83.1	31.6	25.9	27.3
x=-3	10º	31.8	31.0	82.2	31.8	26.1	27.0
x=-4	13.5º	32.1	31.2	80.7	32.0	26.3	26.6
x=-5	16.5º	32.1	31.1	78.6	32.1	26.3	26.0
x=-6	20º	31.9	30.7	75.7	31.9	25.9	25.0

IV. LENS PROTOTYPE

The lens was fabricated by milling technique. Each shell was machined separately. The shape of the inner shell allows it to be inserted into the outer shell, Figure 5. They are glued with a very thin resin layer with the same permittivity of Plexiglas. The waveguide feed (Figure 6) is attached to the lens base using a threaded fixture, Figure 7. This strut can slide across a limited range of distances at the base of the lens, enabling to control the feed off-axis position.

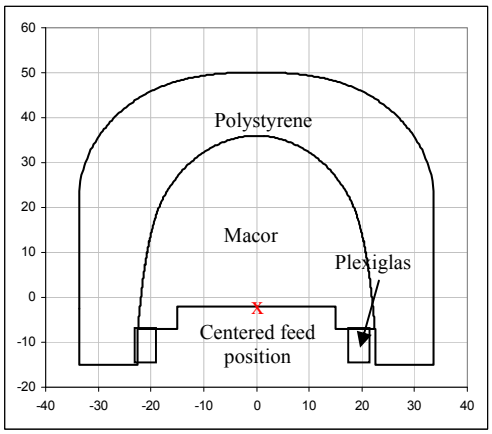

Figure 5. Stand-alone scanning lens, meridional cut.

Figure 6. Fabricated waveguide feed, for 62.5 GHz operation.

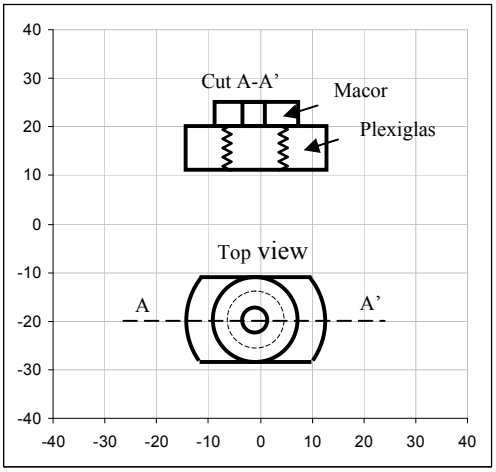

Figure 7. Fixture for waveguide feed.

A photograph of the lens is shown in Figure 8, enabling to see its external profile as well as its bottom part. Being transparent, the outer shell allows seeing the inner shell, although distorted by refraction.

Figure 8. Stand-alone double-shell scanning lens: a) Lens prototype view; b) Strut used to fix the waveguide feed to the lens base.

V. MEASUREMENTS

The measured radiation patterns for the on-axis feed position in the H-plane and E-plane are presented in Figure 9 and Figure 10, respectively. The graphic ordinate scale refers to antenna gain.

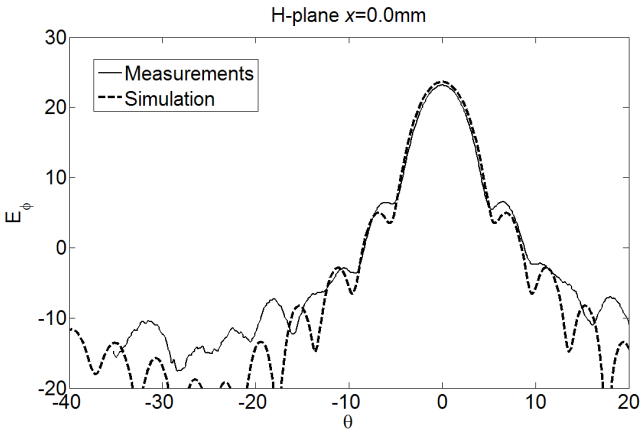

Figure 9. Stand-alone scanning lens H-plane radiation pattern at f = 62.5 GHz; ϕ=0º, 180º cut, with on-axis waveguide feed.

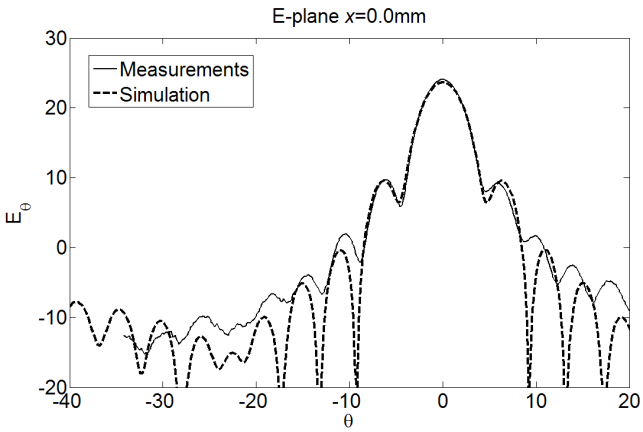

Figure 10. Stand-alone scanning lens E-plane radiation pattern at f = 62.5 GHz; ϕ=90º, 270º cut, with on-axis waveguide feed.

The measured radiation patterns in the H-plane for the different feed displacements are superimposed in Figure 11 to give the overall behavior of the gain scan loss. The agreement between the measured curves and the corresponding ILASH simulated curve is quite good. Minor differences can be attributed to the difficulty to accurately position the feed at the correct off-axis distance, to feed misalignment in the polarization axis and to minor uncertainties in the determination of the materials permittivity. For off-axis feed position, it is observed that the agreement with simulations (especially the first shoulder level) tends to be worse on the side of the lens into which the feed is displaced off from the lens axis. If we go back to the ray tracing of Figure 3, it is seen that a total internal reflection region appears on that side of the lens, which is not completely well accounted by GO/PO because this corresponds to the onset of a surface wave [16]. Note that smaller total internal reflection regions already exist for the on-axis feed case.

Gain increases with off-axis feed displacement because the lens focal arc is not plane and it intersects the lens base near $x = 6\ mm$, as previously mentioned. Again from Figure 3, it is clear that output rays are more parallel for $x = 6\ mm$ than for $x = 0\ mm$. The beam shape is reasonably retained up to $x = 5\ mm$, corresponding to a scan angle of the order of 16º.

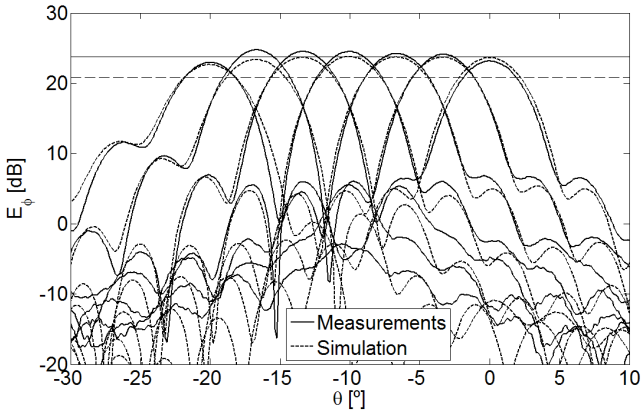

Figure 11. Stand-alone scanning lens (FL2) measured H-plane radiation pattern at f = 62.5 GHz, ϕ = 0º, 180º cuts, for waveguide feed positions x = 0, 1, 2, 3, 4, 5 and 6 mm.

Because radiation pattern phase (and in some cases also phase center position) cannot be measured, a limitation results in the determination of the measured Gaussissity. So, instead of using the expression presented in [17] to determine the Gaussissity we have used instead the following equation:

$$\eta_G = \frac{\left[\iint\left[\bar{u}_P \cdot \bar{E}\right]\exp\left(-\left(\frac{\theta}{\theta_0}\right)^2\right)\sin(\theta)\,d\theta\,d\varphi\right]^2}{\iint\left\|\bar{E}\right\|^2\sin(\theta)\,d\theta\,d\varphi\iint\exp\left(-2\left(\frac{\theta}{\theta_0}\right)^2\right)\sin(\theta)\,d\theta\,d\varphi} \qquad (1)$$

where $\bar{u}_p$ is a unit vector representing the polarization of the Gaussian beam, $\bar{E}$ is the measured electrical field amplitude components and θ_0 is the Gaussian width. This was used with the measured radiation planes for on-axis feed position. The best Gaussissity obtained for this frequency is presented in Table 2.

TABLE II
MEASURED GAUSSISSITY OF THE STAND-ALONE SCANNING LENS AT f = 62.5 GHZ WITH ON-AXIS WAVEGUIDE FEED.

	Measured	Simulated
Gaussian width	4.3º	4.1º
Gaussissity	84.96%	82.96%

The lens input return loss was measured at the waveguide port, and so it includes the feed frequency dependence. The result is shown in Figure 12. The presented characteristic is mainly due to the feed dependence on frequency. This is

confirmed by simulation and by the fact that a shift on the feed position does not affect significantly the frequency response.

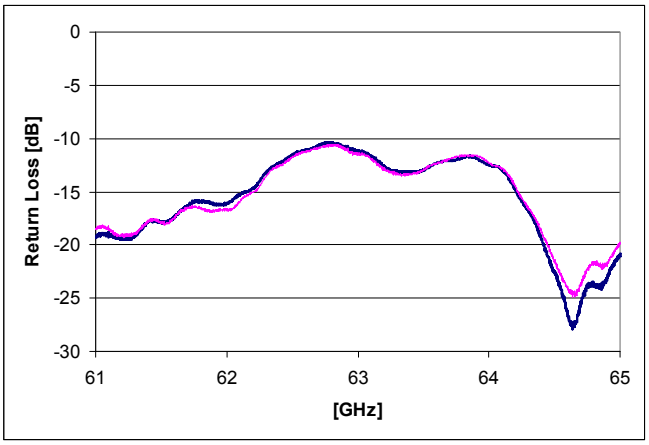

Figure 12. Input return loss of the lens, measured at the waveguide port, for on-axis feed position (blue curve) and for off-axis feed position at x = - 4 mm (pink curve).

VI. Conclusions

This paper presents a double material lens, for stand-alone scanning applications, making use of the closed-form expressions shown in [1], that relate the maximum feed off-axis position with its maximum off-set output angle. The lens beam shape is reasonably retained up to x = 5 mm, corresponding to a scan angle of the order of 16º with a scan gain loss of about 0.5 dB.

Acknowledgment

The authors acknowledge the collaboration from V. Fred and C. Brito for prototype construction, and A. Almeida for prototype measurements.

References

[1] E. B. Lima, J. R. Costa, and C. A. Fernandes, "Design of Double Material Integrated Scanning Lens Antennas", in 2009 IEEE Antennas and Propagation Society International Symposium and USNC/URSI National Radio Science Meeting, Vols 1-6, New York, 2009, pp. 104-107.

[2] C. A. Fernandes, E. B. Lima, and J. R. Costa, "Broadband Integrated Lens for Illuminating Reflector Antenna with Constant Aperture Efficiency", IEEE Trans. Antennas and Propag., vol. 58, pp. 3805-3813, 2010.

[3] J. R. Costa, E. B. Lima, and C. A. Fernandes, "Compact Beam-Steerable Lens Antenna for 60-Ghz Wireless Communications", IEEE Trans. Antennas Propag., vol. 57, pp. 2926-2933, Oct 2009.

[4] N. Ngoc Tinh, N. Delhote, M. Ettorre, D. Baillargeat, L. Le Coq, and R. Sauleau, "Design and Characterization of 60-Ghz Integrated Lens Antennas Fabricated through Ceramic Stereolithography," IEEE Trans. Antennas Propag., vol. 58, pp. 2757-2762, 2010.

[5] J. R. Costa, C. A. Fernandes, G. Godi, R. Sauleau, L. Le Coq, and H. Legay, "Compact Ka-band Lens Antennas for LEO Satellites", IEEE Trans. Antennas Propag., pp. 1251-1268, vol. 56, no. 6, May 2008.

[6] A. Neto, "UWB, Non Dispersive Radiation From the Planarly Fed Leaky Lens Antenna— Part 1: Theory and Design", IEEE Trans. Antennas Propag.,pp. 2238-2247, vol. 58, no. 7, July 2010.

[7] A. Neto, "UWB, Non Dispersive Radiation From the Planarly Fed Leaky Lens Antenna— Part II: Demonstrators and Measurements", IEEE Trans. Antennas Propag.,pp. 2248-2258, vol. 58, no. 7, July 2010.

[8] A. V. Boriskin, R. Sauleau, A.I. Nosich, "Lens Shaping aimed at improvement of the beam-switching antenna off-axis properties", Proc European Conf. on Antennas & Propagation - EUCAP, Edinburgh, United Kingdom, , November, 2007.

[9] L. Xue, V. Fusco, "Patch Fed Planar Dielectric Slab Extended Hemi-Elliptical Lens Antenna", IEEE Trans Antennas Propag., vol. 56, no. 3, pp. 661-666, March 2008.

[10] D. Filipovic, G. Gauthier, S. Raman, and G. Rebeiz, "Off-axis properties of silicon and quartz dielectric lens antennas," IEEE Trans. Antennas Propag., vol. 45, no. 5, pp. 760–766, May 1997.

[11] A. Lamminen, J. Säily, R. Sauleau, and N.-T. Nguyen, "Beam-switching lens antenna at 60 GHz for gigabit data rate wireless indoor connections," in the 5th ESA Workshop on Millimeter Wave Technologies and Applications & 31st ESA Antenna Workshop, ESA/ESTEC, Noordwijkm, The Netherlands, May 2009.

[12] X. Wu, G. Eleftheriades, and T. Van Deventer-Perkins, "Design and characterization of single- and multiple-beam mm-wave circularly polarized substrate lens antennas for wireless communications," IEEE Trans. Microw. Theory Tech., vol. 49, no. 3, pp. 431–441, Mar. 2001.

[13] J. R. Costa, M. G. Silveirinha, and C. A. Fernandes, "Evaluation of a Double-Shell Integrated Scanning Lens Antenna," IEEE Antennas Wirel. Propag. Lett., vol. 7, pp. 781-784, 2008.

[14] M. Born and E. Wolf, Principles of Optics. New York: Pergamon, 1959.

[15] E. Lima, J. Costa, M. Silveirinha, and C. Fernandes, "ILASH—Software tool for the design of integrated lens antennas," Proc. IEEE Antennas Propag. Soc. Int. Symp., San Diego, CA, USA, Jul. 2008.

[16] D. Pasqualini and S. Maci, "High-frequency analysis of integrated dielectric lens antennas," IEEE Trans. Antennas Propag., vol. 52, no. 3, pp. 40–847, Mar. 2004.

[17] D. Filipovic, S. Gearheart, G. Rebeiz; "Double-Slot Antennas on Extended Hemispherical and Elliptical Silicon Dielectric Lenses; IEEE Trans. Microwave Theory and Tech., Vol. 41, No.10, 1738-1749, Oct 1993.